

Neural Clamping: Joint Input Perturbation and Temperature Scaling for Neural Network Calibration

Anonymous authors

Paper under double-blind review

Abstract

Neural network calibration is an essential task in deep learning to ensure consistency between the confidence of model prediction and the true correctness likelihood. In this paper, we propose a new post-processing calibration method called **Neural Clamping**, which employs a simple joint input-output transformation on a pre-trained classifier via a learnable universal input perturbation and an output temperature scaling parameter. Moreover, we provide theoretical explanations on why Neural Clamping is provably better than temperature scaling. Evaluated on BloodMNIST, CIFAR-100, and ImageNet image recognition datasets and a variety of deep neural network models, our empirical results show that Neural Clamping significantly outperforms state-of-the-art post-processing calibration methods. The code is available at anonymous.4open.science/r/NCToolkit.

1 Introduction

Deep neural networks have been widely deployed in real-world machine learning empowered applications such as computer vision, natural language processing, and robotics. However, without further calibration, their confidence made by model prediction usually deviates from the true correctness likelihood (Guo et al., 2017). The issue of poor calibration in neural networks is further amplified in high-stakes or safety-critical decision making scenarios requiring accurate uncertainty quantification and estimation, such as disease diagnosis (Jiang et al., 2012; Esteva et al., 2017) and traffic sign recognition systems in autonomous vehicles (Shafaei et al., 2018). Therefore, calibration plays an important role in trustworthy machine learning (Guo et al., 2017; Kumar et al., 2019; Minderer et al., 2021).

Recent studies on neural network calibration can be mainly divided into two categories: *in-processing* and *post-processing*. In-processing involves training or fine-tuning neural networks to mitigate their calibration errors, such as in Müller et al. (2019); Liang et al. (2020); Tian et al. (2021). Post-processing involves post-hoc intervention on a pre-trained neural network model without changing the given model parameters, such as adjusting the data representations of the penultimate layer (i.e., the logits) to calibrate the final softmax layer’s output of prediction probability estimates. As in-processing calibration tends to be time-consuming and computationally expensive, in this paper, we opt to focus on post-processing calibration.

Current post-processing calibration methods are predominately shed on processing or remapping the output logits of neural networks, *e.g.*, Guo et al. (2017); Kull et al. (2019); Gupta et al. (2020); Tian et al. (2021). However, we aim to provide a new perspective and show that joint input-output model calibration can further improve neural network calibration. The rationale is that active adjustment of data inputs will affect their representations in every subsequent layer, rather than passive modification of the output logits.

In this paper, we propose a new post-processing calibration framework for neural networks. We name this framework **Neural Clamping** because its methodology is based on learning a simple joint input-output transformation for calibrating a pre-trained (frozen) neural network classifier. Figure 1 illustrates the entire procedure of Neural Clamping. We consider a K -way neural network classifier $f_{\theta}(\cdot) \in \mathbb{R}^K$ with fixed model parameters θ . The classifier outputs the logits for K classes and uses softmax on the logits to obtain the final confidence on class predictions (i.e., probability scores). To realize joint input-output calibration, Neural Clamping adds a trainable universal perturbation δ to every data input and a trainable temperature scaling

parameter T at the output logits. The parameters δ and T are jointly learned by minimizing the focal loss Lin et al. (2017) with a weight-decay regularization term trained on a calibration set $\{x_i, y_i\}_{i=1}^n$ for calibration. The focal loss assigns non-uniform importance on $\{x_i\}_{i=1}^n$ during training and includes the standard cross entropy loss as a special case. Finally, in the evaluation (testing) phase, Neural Clamping appends the optimized calibration parameters δ^* and T^* to the input and output of the fixed classifier $f_\theta(\cdot)$, respectively.

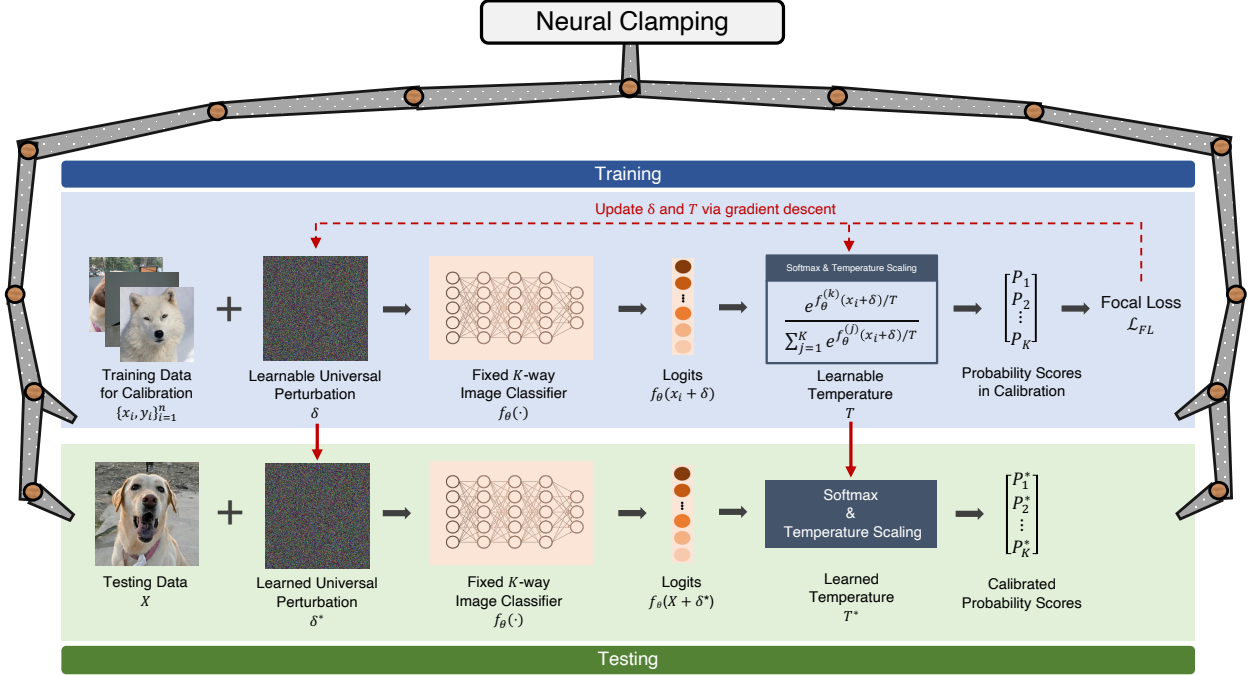


Figure 1: Overview of Neural Clamping: a joint input-output post-processing calibration framework.

Our main contributions are summarized as follows:

- We propose Neural Clamping as a novel joint input-output post-processing calibration framework for neural networks. Neural Clamping learns a universal input perturbation and a temperature scaling parameter at the model output for calibration. It includes temperature scaling as a special case, which is a strong baseline for post-processing calibration.
- We develop theoretical results to prove that Neural Clamping is better than temperature scaling in terms of constrained entropy maximization for uncertainty quantification. In addition, we use first-order approximation to optimize the data-driven initialization term for the input perturbation, improving the stability of Neural Clamping in our ablation study. Furthermore, we leverage this theoretical result to design a computationally efficient algorithm for Neural Clamping.
- Evaluated on different deep neural network classifiers (including ResNet (He et al., 2016), Vision Transformers (Dosovitskiy et al., 2020), and MLP-Mixer (Tolstikhin et al., 2021)) trained on Blood-MNIST (Yang et al., 2023), CIFAR-100 (Krizhevsky et al., 2009), and ImageNet-1K (Deng et al., 2009) datasets and three calibration metrics, Neural Clamping outperforms state-of-the-art post-processing calibration methods. For instance, when calibrating the ResNet-110 model on CIFAR-100, the expected calibration error is improved by 34% when compared to the best baseline.

2 Background and Related Work

In this section, we begin by introducing the problem formulation for calibration and describing the notations used in this paper. Furthermore, we define different metrics used to measure calibration error and conclude this section with an overview of the post-processing calibration methods.

2.1 Probabilistic Characterization of Neural Network Calibration

Assume a pair of data sample and label (\mathbf{x}, y) is drawn from a joint distribution $\mathcal{D} \subset \mathbb{X} \times \mathbb{Y}$, where $\mathbf{x} \in \mathbb{X}$ is a data sample, and $y \in \mathbb{Y} = \{1, \dots, K\}$ is the ground-truth class label. Let $f_\theta : \mathcal{X} \rightarrow \mathbb{R}^K$ denote a K -way neural network classifier parametrized by θ , where $\mathbf{z} = f_\theta(\mathbf{x}) = [z_1, \dots, z_K]$ is the model's output *logits* of a given data input \mathbf{x} . Following the convention of neural network implementations, the prediction probability score of \mathbf{x} is obtained by applying the *softmax* function σ on \mathbf{z} , denoted as $\sigma(\mathbf{z}) \in [0, 1]^K$. The k -th component of $\sigma(\mathbf{z})$ is defined as $\sigma(\mathbf{z})_k = \exp(z_k) / \sum_{k'=1}^K \exp(z_{k'})$, which satisfies $\sum_{k=1}^K \sigma(\mathbf{z})_k = 1$ and $\sigma(\mathbf{z})_k \geq 0$. Suppose the model predicts a most likely class $\hat{y} = \arg \max_k \sigma(\mathbf{z})_k$ with confidence $\hat{p} = \sigma(\mathbf{z})_{\hat{y}}$. Formally, the model f_θ is called *calibrated* if

$$\mathbb{P}(y = \hat{y} | p = \hat{p}) = \hat{p}, \quad (1)$$

where \mathbb{P} denotes probability and p denotes the true likelihood. Equation (1) only considers the prediction confidence of the most likely (top-1) class. We can extend it to consider the prediction confidence of every class. Let the class-wise prediction confidence be $\hat{p}_i = \sigma(\mathbf{z})_i$ for $i = \{1, \dots, K\}$, the network is called *classwise-calibrated* if

$$\mathbb{P}(y = i | p_i = \hat{p}_i) = \hat{p}_i, \quad \forall i \in \mathbb{Y} \quad (2)$$

where p_i is the true likelihood for class i .

2.2 Calibration Metrics

Expected Calibration Error (ECE). Calibration error aims to compute the difference between confidence and accuracy as

$$\mathbb{E}_{(x,y) \sim \mathcal{D}} [|\mathbb{P}(y = \hat{y} | p = \hat{p}) - \hat{p}|] \quad (3)$$

Unfortunately, this quantity cannot be exactly computed from equation (3) if the underlying data distribution \mathbb{D} is unknown. The most popular metric to measure calibration is the *Expected Calibration Error* (ECE) (Guo et al., 2017; Naeini et al., 2015). ECE approximates the calibration error by partitioning predictions into m intervals (bins) $\{B_i\}_{i=1}^m$. The calibration error is calculated by first taking the difference between the confidence and accuracy in each bin and then computing the weighted average across all bins, i.e.,

$$\text{ECE} = \sum_{i=1}^M \frac{|B_i|}{n} |\text{acc}(B_i) - \text{conf}(B_i)| \quad (4)$$

where $|B_i|$ is the number of samples in bin B_i , n is the total number of data, and $\text{acc}(B_i)$ and $\text{conf}(B_i)$ is the accuracy and confidence in B_i , respectively.

Adaptive Expected Calibration Error (AECE) (Mukhoti et al., 2020). Since most data for a trained model fall into the highest confidence bins, these bins mostly determine the value of the ECE. Instead of pre-defined intervals for bin partitioning, in AECE, adaptive interval ranges ensure each bin has the same number of samples. AECE is defined as

$$\begin{aligned} \text{AECE} &= \sum_{i=1}^M \frac{|B_i|}{n} |\text{acc}(B_i) - \text{conf}(B_i)| \\ &\text{subject to } |B_i| = |B_j| \quad \forall i, j \end{aligned} \quad (5)$$

where $|B_i|$ is the number of samples in bin B_i , n is the total number of data, and $\text{acc}(B_i)$ and $\text{conf}(B_i)$ is the accuracy and confidence in B_i , respectively.

Static Calibration Error (SCE) (Nixon et al., 2019). ECE does not take into account the calibration error for all classes. It only calculates the calibration error of the top-1 class prediction. SCE extends ECE and considers multi-class predictions based on Equation (2):

$$\text{SCE} = \frac{1}{K} \sum_{k=1}^K \sum_{i=1}^M \frac{|B_i^k|}{n} |\text{acc}(i, k) - \text{conf}(i, k)| \quad (6)$$

where K is the number of classes, $|B_i^k|$ is the number of samples in bin i of class k , n is the total number of data, and $\text{acc}(i, k)$ and $\text{conf}(i, k)$ is the accuracy and confidence in B_i^k , respectively.

2.3 Post-Processing Calibration Methods

Temperature Scaling (Guo et al., 2017). Temperature scaling is the simplest variant of Platt scaling (Platt et al., 1999), which is a method of converting a classifier’s output into a probability distribution over all classes. Specifically, all classes have the same scalar parameter (i.e., temperature) $T > 0$ in the softmax output such that $\hat{\mathbf{q}} = \sigma(\mathbf{z}/T)$, where $\hat{\mathbf{q}} \in [0, 1]^K$ denotes the calibrated probability scores. It is worth noting that by definition temperature scaling only changes the confidence but not the class prediction. Moreover, the entropy of $\hat{\mathbf{q}}$ increases with T when $T \geq 1$. The temperature T is optimized via the Negative Log Likelihood (NLL) over a calibration training set $\{\mathbf{x}_i\}_{i=1}^n$, where NLL is defined as $-\sum_{i=1}^n \log(\hat{q}_{i, y_i})$ and \hat{q}_{i, y_i} is the prediction on the correct class y_i for the i -th sample.

Vector Scaling and Matrix Scaling (Guo et al., 2017). They are two extensions of Platt scaling (Platt et al., 1999). Let \mathbf{z} be the output logits for an input \mathbf{x} . Vector Scaling and Matrix Scaling adopt linear transformations on \mathbf{z} such that $\hat{\mathbf{q}} = \sigma(\mathbf{W}\mathbf{z} + \mathbf{b})$, where $\mathbf{W} \in \mathbb{R}^{K \times K}$ and $\mathbf{b} \in \mathbb{R}^K$ for both settings. Vector scaling is a variation of matrix scaling when \mathbf{W} is restricted to be a diagonal matrix. The parameters \mathbf{W} and \mathbf{b} are optimized based on NLL.

MS-ODIR and Dir-ODIR (Kull et al., 2019). The authors in Kull et al. (2019) proposed Dirichlet calibration and ODIR term (Off-Diagonal and Intercept Regularization). The difference between matrix scaling and Dirichlet calibration is that the former affects logits while the latter modifies pseudo-logits through $\hat{\mathbf{q}} = \sigma(\mathbf{W} \ln(\sigma(\mathbf{z})) + \mathbf{b})$, where $\ln(\cdot)$ is a component-wise natural logarithm function. The results in Guo et al. (2017) indicated poor matrix scaling performance, because calibration methods with a large number of parameters will over-fit to a small calibration set. Therefore, Kull et al. (2019) proposed a new regularization method called ODIR to address the overfitting problem, i.e. $\text{ODIR} = \frac{1}{K(K-1)} \sum_{j \neq k} w_{j,k} + \frac{1}{K} \sum_j b_j$, where $w_{j,k}$ and b_j are elements of \mathbf{W} and \mathbf{b} , respectively. MS-ODIR applies Matrix Scaling (Guo et al., 2017) with ODIR, while Dir-ODIR uses Dirichlet calibration (Kull et al., 2019).

Spline-Fitting (Gupta et al., 2020). Spline-fitting approximates the empirical cumulative distribution with splines to re-calibrate network outputs for calibrated probabilities. However, this method is limited to calibration on the top- k class prediction but cannot be extended to all-class predictions. Therefore, this method is beyond our studied problem of all-class post-processing calibration.

3 Neural Clamping

Based on the proposed framework of Neural Clamping as illustrated in Figure 1, in this section we provide detailed descriptions on the joint input-output calibration methodology, the training objective function, the influence of hyperparameter selection, and the theoretical justification on the improvement over temperature scaling and the data-driven initialization.

3.1 Joint Input-Output Calibration

To realize joint input-output calibration, Neural Clamping appends a learnable universal perturbation δ at the model input and a learnable temperature scaling parameter T for all classes at the model output. In contrast to the convention of output calibration, Neural Clamping introduces the notion of input calibration by applying simple trainable transformations on the data inputs prior to feeding them to the model. In our implementation, the input calibration is simply a universal additive perturbation δ . Therefore, Neural Clamping includes temperature scaling as a special case when setting $\delta = 0$.

Modern neural networks often suffer from an overconfident issue, resulting in a lack of well-calibration and low output entropy (Guo et al., 2017; Mukhoti et al., 2020). Calibrating neural networks, a common approach to address the overconfident issue, typically results in increased entropy as a byproduct. In the seminal work on neural network calibration by Guo et al. (2017), it is noted that adjusting the temperature parameter to

improve calibration aligns with the objective of maximizing the entropy of the output probability distribution under additional constraints.

Building upon this notion, we extend the problem formulation presented in Guo et al. (2017), which utilizes entropy to study output calibration. We evaluate this problem on a calibration set $\{\mathbf{x}_i, y_i\}_{i=1}^n$ with an input perturbation δ . The objective is to find the best-calibrated output q^* that maximizes the entropy of q^* while satisfying the specified calibration constraints:

$$\begin{aligned} & \text{Maximize}_{q \in \mathbb{R}^K} - \sum_{i=1}^n q(\mathbf{z}_i)^\top \log(q(\mathbf{z}_i)) \\ & \text{subject to } q(\mathbf{z}_i)^{(k)} \geq 0 \quad \forall i \in \{1, \dots, n\} \text{ and } k \in \{1, \dots, K\} \\ & \sum_{i=1}^n \mathbf{1}^\top q(\mathbf{z}_i) = 1 \\ & \sum_{i=1}^n \mathbf{z}_i^\top \mathbf{e}^{(y_i)} = \sum_{i=1}^n \mathbf{z}_i^\top q(\mathbf{z}_i) \end{aligned} \quad (7)$$

where \cdot^\top denotes vector transpose, $\mathbf{z}_i = f_\theta(\mathbf{x}_i + \delta)$ is the logit of $\mathbf{x}_i + \delta$, $\mathbf{1}$ is an all-one vector, $\mathbf{e}^{(y_i)}$ is an one-hot vector corresponding to the class label y_i , and $\log(\cdot)$ is an element-wise log operator. The first two constraints guarantee that q is a probability distribution, whereas the third constraint restricts the range of possible distributions, which stipulates that the average true class logit equals to the average weighted logit.

To motivate the utility of joint input-output calibration, the following lemma formally states that the proposed form of joint input perturbation and temperature scaling in Neural Clamping is the unique solution q^* to the above constrained entropy maximization problem.

Lemma 3.1 (optimality of joint input-output calibration). *For any input perturbation δ , let $f_\theta(\cdot) = [f_\theta^{(1)}, \dots, f_\theta^{(K)}]$ be a fixed K -way neural network classifier and let \mathbf{z} be the output logits of a perturbed data input $\mathbf{x} + \delta$. Then the proposed form of joint input-output calibration in Neural Clamping is the unique solution $q^*(z)^{(k)} = \frac{\exp[f_\theta^{(k)}(\mathbf{x} + \delta)/T]}{\sum_{j=1}^K \exp[f_\theta^{(j)}(\mathbf{x} + \delta)/T]}$, $\forall k \in \{1, \dots, K\}$, to the constrained entropy maximization problem in equation 7.*

Proof. The proof is given in Appendix B.

3.2 Training Objective Function in Neural Clamping

Neural Clamping uses the focal loss (Lin et al., 2017) and a weight-decay regularization term as the overall objective function for calibration. It has been shown that the focal loss is an upper bound of the regularized KL-divergence (Charoenphakdee et al., 2021; Mukhoti et al., 2020). Therefore, minimizing the focal loss aims to reduce the KL divergence between the groundtruth distribution and the predicted distribution while increasing the entropy of the predicted distribution. Focal loss is an adjusted cross entropy loss with a modulating factor $(1 - \hat{p}_{i,y_i})^\gamma$ and $\gamma \geq 0$, where \hat{p}_{i,y_i} is the prediction probability given by a neural network on the correct class y_i for the i -th sample. When $\gamma = 0$, focal loss reduces to the standard cross entropy loss. Formally, it is defined as

$$\mathcal{L}_{FL}^\gamma(f_\theta(\mathbf{x}_i), y_i) = -(1 - \hat{p}_{i,y_i})^\gamma \log(\hat{p}_{i,y_i}) \quad (8)$$

Given a calibration training set $\{\mathbf{x}_i, y_i\}_{i=1}^n$, the optimal calibration parameters δ and T in Neural Clamping are obtained by solving

$$\delta^*, T^* = \arg \min_{\delta, T} \sum_{i=1}^n \mathcal{L}_{FL}^\gamma(f_\theta(\mathbf{x}_i + \delta)/T, y_i) + \lambda \|\delta\|_2^2 \quad (9)$$

Like other post-processing calibration methods, Neural Clamping only appends a perturbation at the model input and a temperature scaling parameter at the model output. It does not require any alternations on the given neural network for calibration.

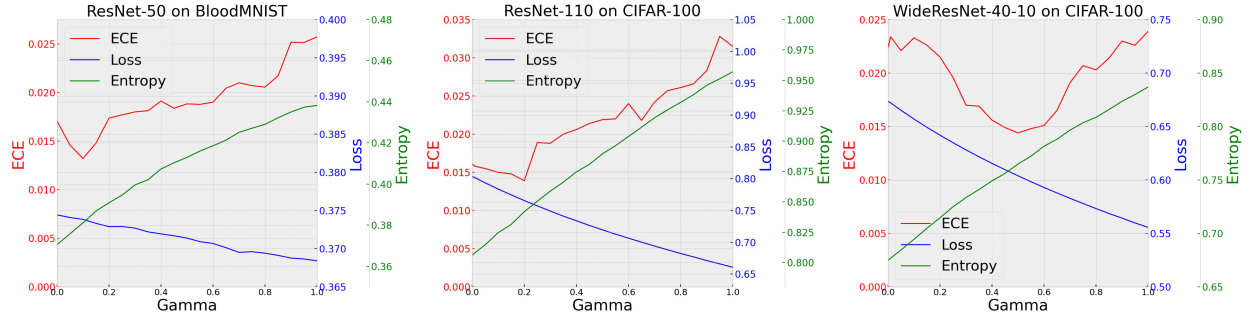


Figure 2: Neural Clamping on ResNet-50/ResNet-110 and Wide-ResNet-40-10 with different γ values and the resulting expected calibration error (ECE), training loss, and entropy on BloodMNIST and CIFAR-100. When $\gamma = 0$, focal loss reduces to cross entropy loss. The experiment setup is the same as Section 4.

3.3 How to Choose a Proper γ Value in Focal Loss for Neural Clamping?

The focal loss has a hyperparameter γ governing the assigned importance on each data sample in the aggregated loss. To understand its influence on calibration, in Figure 2 we performed a grid search of γ value between 0 and 1 with an interval of 0.05 to calibrate Wide-Resnet-40-10 (Zagoruyko & Komodakis, 2016) and DenseNet-121 (Huang et al., 2017) models trained on CIFAR-100 (Krizhevsky et al., 2009) dataset. While the entropy continues to increase as the gamma value increases, ECE attains its minimum at some intermediate γ value and is better than the ECE of using cross entropy loss (i.e., $\gamma = 0$). This observation verifies the importance of using focal loss for calibration. In our implementation, we select the best γ value that minimizes ECE of the calibration dataset from a candidate pool of γ values with separate runs.

3.4 Theoretical Justification on the Advantage of Neural Clamping

Here we use the entropy after calibration as a quantifiable metric to prove that Neural Clamping can further increase this quantity over temperature scaling. Note that temperature scaling is a special case of Neural Clamping when there is no input calibration (i.e., setting $\delta = 0$). For ease of understanding, we define g_i as the gradient of the output entropy $H(\sigma(f_\theta(\cdot)/T))$ with respect to the input data $\mathbf{x}_i = [x_i^{(1)}, \dots, x_i^{(m)}] \in [\alpha, \beta]$, where $[\alpha, \beta] \subset \mathbb{R}^m \times \mathbb{R}^m$ means the bounded range of all feasible data inputs (e.g., every image pixel value is within $[0, 255]$). We further define $\ell \in \mathbb{R}^m$ and $\mu \in \mathbb{R}^m$ as the lower bound and the upper bound over all calibration data $\{x_i\}_{i=1}^n$ on each input dimension. That is, their j -th entry is defined as $\ell_j = \min_{i \in \{1, \dots, n\}} x_i^{(j)}$ and $\mu_j = \max_{i \in \{1, \dots, n\}} x_i^{(j)}$, respectively.

With the use of first-order approximation, the following theorem shows that given the same temperature value T , Neural Clamping increases the entropy of temperature scaling by $\delta^\top \mathbf{g}$, demonstrating the advantage of involving input calibration. Furthermore, based on our derivation and the data-driven bounds ℓ and μ , we can obtain a closed-form first-order optimal solution $\tilde{\delta}$ for maximizing the entropy increment $\delta^\top \mathbf{g}$. We call $\tilde{\delta}$ the *data-driven initialization* for the input perturbation δ . We will perform an ablation study to compare the performance and stability of data-driven versus random initialization in Section 4.3. In the following theorem, the notation $|\cdot|$, sign , and \odot denote element-wise absolute value, sign operation (i.e., ± 1), and product (i.e., Hadamard product), respectively.

Theorem 3.2. (provable entropy increment and data-driven initialization) *Let $[\alpha, \beta]$ be the feasible range of data inputs and $\mathbf{g} = \sum_{i=1}^n g_i = [g^{(1)}, \dots, g^{(K)}]$ be the sum of local input gradients. Define $\boldsymbol{\eta} \in \mathbb{R}^m$ element-wise such that $\eta_j = \ell_j - \alpha_j$ if $g^{(j)} < 0$, $\eta_j = \beta_j - \mu_j$ if $g^{(j)} > 0$, and $\eta_j = 0$ otherwise, for every $j \in \{1, \dots, m\}$. Approaching by first-order approximation and given the same temperature value T , Neural Clamping increases the entropy of temperature scaling by $\delta^\top \mathbf{g}$. Furthermore, the optimal value $\tilde{\delta}$ for maximizing $\delta^\top \mathbf{g}$ is $\tilde{\delta} = \text{sign}(\mathbf{g}) \odot \boldsymbol{\eta}$.*

Proof. The proof is given in Appendix C.

Table 1: Comparison with various calibration methods on BloodMNIST with ResNet-50. The reported results are mean and standard deviation over 5 runs. The best/second-best method is highlighted by blue/green color. On ECE/AECE, the relative improvement of Neural Clamping to the best baseline is 31% and 28%, respectively.

ResNet-50					
Method	Accuracy (%)	Entropy \uparrow	ECE (%) \downarrow	AECE (%) \downarrow	SCE ($\times 10^{-2}$) \downarrow
Uncalibration	85.79	0.2256	5.77	5.76	1.7003
Temperature Scaling	85.79 ± 0	0.3726 ± 0	1.77 ± 0	1.66 ± 0	1.1067 ± 0
TS by Grid Search	85.79 ± 0	0.3684 ± 0	2.13 ± 0	1.68 ± 0	1.1041 ± 0
Vector Scaling	85.79 ± 0.05	0.3653 ± 0.0023	1.97 ± 0.11	1.94 ± 0.06	0.9264 ± 0.0574
Matrix Scaling	85.79 ± 0.38	0.2984 ± 0.0161	4.96 ± 0.65	4.86 ± 0.71	1.4665 ± 0.1314
MS-ODIR	85.79 ± 0.04	0.3726 ± 0.0001	1.94 ± 0.01	1.70 ± 0.03	0.9099 ± 0.0101
Dir-ODIR	85.79 ± 0.02	0.3748 ± 0.0002	1.55 ± 0.04	1.71 ± 0.09	0.8366 ± 0.0034
Neural Clamping (CE)	85.79 ± 0.02	0.3820 ± 0.0005	1.54 ± 0.02	1.57 ± 0.05	1.1100 ± 0.0103
Neural Clamping (FL)	85.82 ± 0.03	0.4204 ± 0.0004	1.05 ± 0.03	1.19 ± 0.06	1.0797 ± 0.0042

Table 2: Comparison with various calibration methods on CIFAR-100 with different models. The reported results are mean and standard deviation over 5 runs. The best/second-best method is highlighted by blue/green color. On ECE, the relative improvement of Neural Clamping to the best baseline is 34/5 % on ResNet-110/Wide ResNet-40-10, respectively.

ResNet-110					
Method	Accuracy (%)	Entropy \uparrow	ECE (%) \downarrow	AECE (%) \downarrow	SCE ($\times 10^{-2}$) \downarrow
Uncalibration	74.15	0.4742	10.74	10.71	0.2763
Temperature Scaling	74.15 ± 0	0.8991 ± 0	1.71 ± 0	1.63 ± 0	0.1711 ± 0
TS by Grid Search	74.15 ± 0	0.9239 ± 0	1.35 ± 0	1.38 ± 0	0.1717 ± 0
Vector Scaling	73.81 ± 0.05	0.8698 ± 0.0008	2.29 ± 0.07	2.15 ± 0.15	0.1949 ± 0.0046
Matrix Scaling	62.03 ± 0.31	0.1552 ± 0.0026	31.85 ± 0.29	31.85 ± 0.29	0.6842 ± 0.0057
MS-ODIR	74.07 ± 0.03	0.9035 ± 0.0001	1.79 ± 0.04	1.75 ± 0.03	0.1797 ± 0.0006
Dir-ODIR	74.10 ± 0.04	0.9160 ± 0.0002	1.36 ± 0.05	1.31 ± 0.03	0.1780 ± 0.0014
Neural Clamping (CE)	74.17 ± 0.07	0.8928 ± 0.0061	1.67 ± 0.16	1.63 ± 0.19	0.1709 ± 0.0020
Neural Clamping (FL)	74.16 ± 0.09	0.9707 ± 0.0049	0.89 ± 0.06	1.01 ± 0.11	0.1754 ± 0.0015
Wide-ResNet-40-10					
Method	Accuracy (%)	Entropy \uparrow	ECE (%) \downarrow	AECE (%) \downarrow	SCE ($\times 10^{-2}$) \downarrow
Uncalibration	79.51	0.4210	7.63	7.63	0.2188
Temperature Scaling	79.51 ± 0	0.7420 ± 0	2.30 ± 0	2.17 ± 0	0.1627 ± 0
TS by Grid Search	79.51 ± 0	0.8359 ± 0	1.75 ± 0	1.54 ± 0	0.1659 ± 0
Vector Scaling	79.08 ± 0.09	0.7079 ± 0.0012	2.52 ± 0.07	2.35 ± 0.05	0.1818 ± 0.0032
Matrix Scaling	68.48 ± 0.16	0.1371 ± 0.0023	26.13 ± 0.15	26.12 ± 0.15	0.5657 ± 0.0024
MS-ODIR	79.15 ± 0.03	0.7529 ± 0.0002	1.90 ± 0.07	1.95 ± 0.03	0.1705 ± 0.0008
Dir-ODIR	79.51 ± 0.01	0.7707 ± 0.0001	1.81 ± 0.03	1.98 ± 0.01	0.1625 ± 0.0004
Neural Clamping (CE)	79.53 ± 0.01	0.7461 ± 0.0030	2.27 ± 0.03	2.20 ± 0.03	0.1624 ± 0.0004
Neural Clamping (FL)	79.53 ± 0.04	0.8626 ± 0.0033	1.67 ± 0.14	1.66 ± 0.12	0.1683 ± 0.0014

4 Performance Evaluation

In this section, we conducted extensive experiments to evaluate the performance of our proposed Neural Clamping calibration method using the calibration metrics introduced in Section 2.2. We compared our method to several baseline and state-of-the-art calibration methods. All experiments are evaluated on three popular image recognition datasets (BloodMNIST, CIFAR100, ImageNet-1K) and six trained deep neural network models (e.g. ResNet, Vision Transformer (ViT), and MLP-Mixer). An ablation study on Neural Clamping is presented at the end of this section.

4.1 Evaluation and Implementation Details

Experiment setup. We used ResNet-50 (He et al., 2016) on BloodMNIST (Yang et al., 2023); ResNet-110 (He et al., 2016) and Wide-ResNet-40-10 (Zagoruyko & Komodakis, 2016) models on CIFAR-100 (Krizhevsky et al., 2009); ResNet-101 (He et al., 2016), ViT-S/16 (Dosovitskiy et al., 2020), and MLP-Mixer B/16

Table 3: Comparison with various calibration methods on ImageNet with different models. The reported results are mean and standard deviation over 5 runs. The best/second-best method is highlighted by blue/green color. On ECE, the relative improvement of Neural Clamping to the best baseline is 11/6/13 % on ResNet-101/ViT-S16/MLP-Mixer B16, respectively.

ResNet-101					
Method	Accuracy (%)	Entropy \uparrow	ECE (%) \downarrow	AECE (%) \downarrow	SCE ($\times 10^{-3}$) \downarrow
Uncalibration	75.73	0.6608	5.88	5.88	0.3180
Temperature Scaling	75.73 ± 0	0.9376 ± 0	1.88 ± 0	1.91 ± 0	0.3117 ± 0
TS by Grid Search	75.73 ± 0	0.9244 ± 0	2.02 ± 0	1.97 ± 0	0.3108 ± 0
Vector Scaling	75.67 ± 0.07	1.0463 ± 0.0017	2.04 ± 0.12	1.92 ± 0.07	0.3192 ± 0.0009
Matrix Scaling	51.97 ± 0.30	0.0593 ± 0.0008	45.61 ± 0.28	45.60 ± 0.28	0.9037 ± 0.0052
MS-ODIR	70.71 ± 0.10	0.9904 ± 0.0016	3.29 ± 0.06	3.28 ± 0.06	0.3448 ± 0.0011
Dir-ODIR	70.72 ± 0.03	0.9841 ± 0.0007	3.47 ± 0.05	3.47 ± 0.05	0.3480 ± 0.0013
Neural Clamping (CE)	75.73 ± 0.01	0.9429 ± 0.0240	1.89 ± 0.13	1.88 ± 0.11	0.3114 ± 0.0007
Neural Clamping (FL)	75.73 ± 0.01	1.0103 ± 0.0245	1.68 ± 0.04	1.71 ± 0.03	0.3128 ± 0.0001
ViT-S/16					
Method	Accuracy (%)	Entropy \uparrow	ECE (%) \downarrow	AECE (%) \downarrow	SCE ($\times 10^{-3}$) \downarrow
Uncalibration	79.90	0.7161	1.28	1.30	0.2808
Temperature Scaling	79.90 ± 0	0.7314 ± 0	1.08 ± 0	1.09 ± 0	0.2817 ± 0
TS by Grid Search	79.90 ± 0	0.7791 ± 0	0.82 ± 0	0.80 ± 0	0.2852 ± 0
Vector Scaling	80.02 ± 0.03	0.9410 ± 0.0014	2.62 ± 0.02	2.69 ± 0.03	0.2985 ± 0.0015
Matrix Scaling	53.99 ± 0.29	0.0646 ± 0.0010	43.36 ± 0.30	43.36 ± 0.29	0.8811 ± 0.0054
MS-ODIR	75.94 ± 0.09	0.9810 ± 0.0018	0.87 ± 0.10	0.92 ± 0.10	0.3163 ± 0.0023
Dir-ODIR	75.93 ± 0.09	0.9788 ± 0.0007	0.93 ± 0.06	0.86 ± 0.09	0.3149 ± 0.0018
Neural Clamping (CE)	79.98 ± 0.01	0.7898 ± 0.0028	0.81 ± 0.03	0.77 ± 0.04	0.2801 ± 0.0005
Neural Clamping (FL)	79.97 ± 0.01	0.7934 ± 0.0038	0.77 ± 0.01	0.72 ± 0.03	0.2804 ± 0.0004
MLP-Mixer B/16					
Method	Accuracy (%)	Entropy \uparrow	ECE (%) \downarrow	AECE (%) \downarrow	SCE ($\times 10^{-3}$) \downarrow
Uncalibration	73.94	0.6812	11.55	11.55	0.3589
Temperature Scaling	73.94 ± 0	1.2735 ± 0	4.94 ± 0	4.98 ± 0	0.3188 ± 0
TS by Grid Search	73.94 ± 0	1.6243 ± 0	2.60 ± 0	2.60 ± 0	0.3258 ± 0
Vector Scaling	73.24 ± 0.06	1.1474 ± 0.0089	6.91 ± 0.17	6.88 ± 0.20	0.3321 ± 0.0027
Matrix Scaling	40.96 ± 0.31	0.1137 ± 0.0010	54.50 ± 0.28	54.50 ± 0.28	1.0979 ± 0.0041
MS-ODIR	73.16 ± 0.02	1.8049 ± 0.0016	4.65 ± 0.08	4.73 ± 0.05	0.3477 ± 0.0018
Dir-ODIR	73.13 ± 0.05	1.8083 ± 0.0013	4.68 ± 0.09	4.76 ± 0.09	0.3480 ± 0.0018
Neural Clamping (CE)	74.14 ± 0.01	1.7952 ± 0.0302	2.43 ± 0.16	2.51 ± 0.18	0.3054 ± 0.0020
Neural Clamping (FL)	74.12 ± 0.00	1.7673 ± 0.0269	2.27 ± 0.13	2.34 ± 0.14	0.3029 ± 0.0018

Table 4: Ablation study with ResNet-110 on CIFAR-100. The best result is highlighted by blue color.

Method	Accuracy (%)	Entropy \uparrow	ECE (%) \downarrow	AECE (%) \downarrow	SCE ($\times 10^{-2}$) \downarrow
No Calibration	74.15	0.4742	10.74	10.71	0.2763
Input Calibration w/ δ^*	74.16 ± 0.09	0.4775 ± 0.03	10.62 ± 0.10	10.61 ± 0.10	0.2776 ± 0.0019
Output Calibration w/ T^*	74.15 ± 0	0.9648 ± 0.46	1.18 ± 0.05	1.35 ± 0.01	0.1731 ± 0.0003
Neural Clamping	74.16 ± 0.09	0.9707 ± 0.49	0.89 ± 0.06	1.01 ± 0.11	0.1754 ± 0.0015

(Tolstikhin et al., 2021) models on ImageNet-1K (Deng et al., 2009). Blood MNIST, a recognized medical machine learning benchmark, features 11,959/1,712/3,421 samples for training/validation/evaluation. For CIFAR-100 and ImageNet, lacking default validation data, we divided CIFAR-100’s training set into 45,000 training images and 5,000 calibration images. For ImageNet, 25,000 test images were reserved for calibration, and the remaining 25,000 were for evaluation. Uniform calibration dataset and test set were shared across all methods. Our experiments ran on an Nvidia Tesla V100 with 32GB RAM and Intel Xeon Gold CPU.

Comparative methods. We compared our method to all the post-processing calibration methods introduced in Section 2.3, including Temperature Scaling (Guo et al., 2017), Vector Scaling, Matrix Scaling, Matrix scaling with ODIR (MS-ODIR) (Kull et al., 2019), and Dirichlet Calibration (Dir-ODIR) (Kull et al., 2019). For temperature scaling, we considered two implementations: (a) learning the temperature by minimizing NLL loss via gradient decent on the calibration dataset, and (b) taking a grid search on temperature over 0 to 5 with a resolution of 0.001 and then reporting the lowest ECE and its corresponding temperature, for which we call TS (Grid Searched). For MS-ODIR and Dir-ODIR, we trained their regularization

coefficient with 7 values from 10^{-2} to 10^4 and chose the best result on the calibration dataset (See Section 4.1 in (Kull et al., 2019)). All methods were trained with 1000 epochs with full-batch gradient descent with learning rate 0.001. In addition to Neural Clamping with the focal loss (FL), we also compared Neural Clamping with the cross entropy (CE) loss.

Neural Clamping implementation. The hyperparameters λ and γ in equation (9) are determined by the best parameter minimizing the ECE on the calibration dataset. The choice of γ was already discussed in Sec 3.3. The default value of γ is set to 1 because we find it to be stable across models and datasets. Regarding the choice of λ , its purpose is to aid in regularization. Our default approach is to set this term to be 1/10 of the initial loss. The input calibration parameter δ and the output calibration parameter T are optimized using the stochastic gradient descent (SGD) optimizer with learning rate 0.001, batch size 512, and 100 epochs. For initialization, δ uses random initialization and T is set to 1. The detailed algorithmic procedure of Neural Clamping is presented in Appendix A.

Evaluation metrics. We reported 5 evaluation measures on the test sets: Accuracy, Entropy, ECE, AECE, and SCE. All three calibration metrics are defined in Section 2.2 and 15 bins were used. In all experiments, we report the average value and standard deviation over 5 independent runs.

4.2 BloodMNIST, CIFAR-100, and ImageNet Results

BloodMNIST. BloodMNIST is an 8-class microscopic peripheral blood cell image recognition task. The calibration results with ResNet-50 are shown in Table 1. Compared to the best existing method, Neural Clamping shows an additional 31%/28% reduction in ECE/AECE.

CIFAR-100. The experimental results on CIFAR-100 are presented in Table 2, which is divided into two sections corresponding to different models: ResNet-110 and Wide-ResNet-40-10. Our method consistently achieves the lowest ECE and either the lowest or second lowest AECE and SCE when compared to other existing methods. Notably, in the ResNet-110 experiment, Neural Clamping reduced ECE and AECE by 34% and 23%, respectively, compared to the best existing method. It is important to highlight that our method not only reduces calibration error but also improves accuracy, which sets it apart from existing approaches.

ImageNet-1K. Table 3 presents the experimental results on ImageNet, where the table is divided into three sections containing ResNet-101, ViT-S/16, and MLP-Mixer B/6. Neural Clamping consistently outperforms the compared methods by achieving the lowest ECE, AECE, and either the lowest or second-lowest SCE in all cases, similar to the CIFAR-100 experiments. Particularly, in the ResNet-101 experiment, Neural Clamping reduces ECE and AECE by 11% compared to the best existing method. Moreover, our method concurrently improves accuracy while reducing the calibration error for all three models, demonstrating its effectiveness in calibration for various model architectures.

Additionally, We also provide experimental results of different bins number in Appendix D, which clearly demonstrates the same conclusion of the outstanding calibration performance of Neural Clamping over the baselines. To further compare how our method differs from the baselines, we also visualize the ECE results via plotting the reliability diagrams in Appendix E.

4.3 Additional Analysis of Neural Clamping

Data-driven vs. random initialization for input perturbation δ . There are two initialization methods for the input calibration δ in Neural Clamping: data-driven initialization as derived from Theorem 3.2 and random initialization. In scrutinizing these two initialization methods, we found that the data-driven initialization managed to consistently deliver stable calibration results. Figure 3 shows that across all metrics, both initialization methods have similar mean values across 5 runs, while the data-driven initialization has a smaller variation and standard deviation. As a result of the experiment, it can be concluded that data-driven value can not only offer a more reliable solution but also slightly improved outcomes. We also used this data-driven initialization to devise a computationally efficient Neural Clamping variant. Under a similar run-time constraint, our approach can attain a better calibration performance than temperature scaling. Please see Appendix F for details.

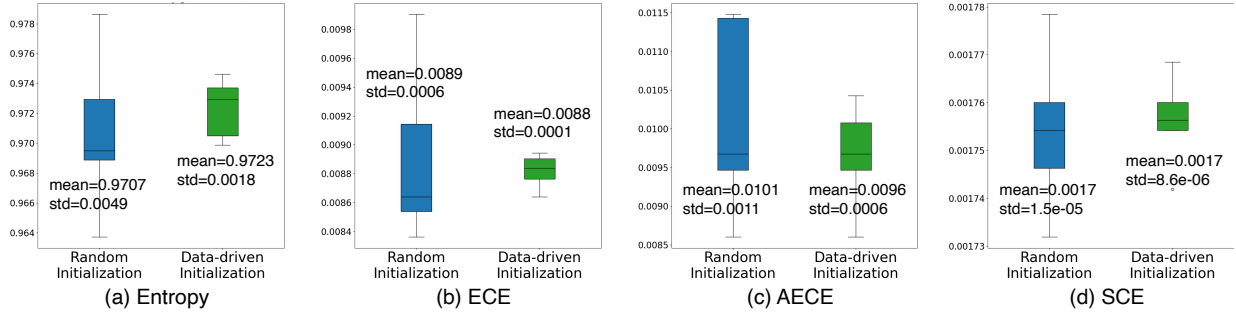


Figure 3: Comparison of random (blue) and data-driven (green) initializations for input calibration δ in Neural Clamping. The reported results are (a) Entropy, (b) ECE, (c) AECE, and (d) SCE of ResNet-110 on CIFAR-100 over 5 runs. This boxplot graphically demonstrates the spread groups of numerical data through their quartiles. The data-driven initialization shows better stability (smaller variation) than random initialization.

Ablation study with input calibration δ^* and output calibration T^* . After calibration, Neural Clamping learns δ^* for input calibration and T^* for output calibration. In Table 4 we performed an ablation study to examine the effects of input calibration and output calibration separately with their jointly trained parameters δ^* and T^* . For input calibration, we inferred testing data with only the learned input perturbation δ^* ; for output calibration, we tested the result with only the learned temperature scaling parameter T^* . One noteworthy finding from this exercise is that while output calibration alone already trims the ECE and AECE materially, a further 25% reduction in ECE and AECE can be achieved when it is paired with input calibration (i.e. Neural Clamping). Input calibration alone is less effective because it does not directly modify the prediction output. This ablation study corroborates the necessity and advantage of joint input-output calibration.

5 Conclusion

In this paper, we present a new post-processing calibration method called Neural Clamping, which offers novel insights into joint input-output calibration and significantly improves calibration performance. We also develop theoretical analysis to justify the advantage of Neural Clamping. Our empirical results on several datasets and models show that Neural Clamping outperforms state-of-the-art post-processing calibration methods. We believe our method delivers a practical tool that can contribute to neural network based technology and applications requiring accurate calibration.

Impact Statements.

We see no ethical or immediate negative societal consequence of our work, and it holds the potential for positive social impacts. By improving the accuracy of machine learning models’ prediction probabilities, our research can benefit various domains.

References

- Nontawat Charoenphakdee, Jayakorn Vongkulbhisal, Nuttapong Chairatanakul, and Masashi Sugiyama. On focal loss for class-posterior probability estimation: A theoretical perspective. In *Proceedings of the IEEE/CVF Conference on Computer Vision and Pattern Recognition*, pp. 5202–5211, 2021.
- Jia Deng, Wei Dong, Richard Socher, Li-Jia Li, Kai Li, and Li Fei-Fei. Imagenet: A large-scale hierarchical image database. In *2009 IEEE conference on computer vision and pattern recognition*, pp. 248–255. Ieee, 2009.
- Alexey Dosovitskiy, Lucas Beyer, Alexander Kolesnikov, Dirk Weissenborn, Xiaohua Zhai, Thomas Unterthiner, Mostafa Dehghani, Matthias Minderer, Georg Heigold, Sylvain Gelly, et al. An image is worth 16x16 words: Transformers for image recognition at scale. *arXiv preprint arXiv:2010.11929*, 2020.

- Andre Esteva, Brett Kopley, Roberto A Novoa, Justin Ko, Susan M Swetter, Helen M Blau, and Sebastian Thrun. Dermatologist-level classification of skin cancer with deep neural networks. *nature*, 542(7639): 115–118, 2017.
- Chuan Guo, Geoff Pleiss, Yu Sun, and Kilian Q Weinberger. On calibration of modern neural networks. In *International Conference on Machine Learning*, pp. 1321–1330. PMLR, 2017.
- Kartik Gupta, Amir Rahimi, Thalaiyasingam Ajanthan, Thomas Mensink, Cristian Sminchisescu, and Richard Hartley. Calibration of neural networks using splines. *arXiv preprint arXiv:2006.12800*, 2020.
- Kaiming He, Xiangyu Zhang, Shaoqing Ren, and Jian Sun. Deep residual learning for image recognition. In *Proceedings of the IEEE conference on computer vision and pattern recognition*, pp. 770–778, 2016.
- Gao Huang, Zhuang Liu, Laurens Van Der Maaten, and Kilian Q Weinberger. Densely connected convolutional networks. In *Proceedings of the IEEE conference on computer vision and pattern recognition*, pp. 4700–4708, 2017.
- Xiaoqian Jiang, Melanie Osl, Jihoon Kim, and Lucila Ohno-Machado. Calibrating predictive model estimates to support personalized medicine. *Journal of the American Medical Informatics Association*, 19(2):263–274, 2012.
- Alex Krizhevsky, Geoffrey Hinton, et al. Learning multiple layers of features from tiny images. 2009.
- Meelis Kull, Miquel Perello Nieto, Markus Kängsepp, Telmo Silva Filho, Hao Song, and Peter Flach. Beyond temperature scaling: Obtaining well-calibrated multi-class probabilities with dirichlet calibration. *Advances in neural information processing systems*, 32, 2019.
- Ananya Kumar, Percy S Liang, and Tengyu Ma. Verified uncertainty calibration. *Advances in Neural Information Processing Systems*, 32, 2019.
- Gongbo Liang, Yu Zhang, Xiaoqin Wang, and Nathan Jacobs. Improved trainable calibration method for neural networks on medical imaging classification. *arXiv preprint arXiv:2009.04057*, 2020.
- Tsung-Yi Lin, Priya Goyal, Ross Girshick, Kaiming He, and Piotr Dollár. Focal loss for dense object detection. In *Proceedings of the IEEE international conference on computer vision*, pp. 2980–2988, 2017.
- Matthias Minderer, Josip Djolonga, Rob Romijnders, Frances Hubis, Xiaohua Zhai, Neil Houlsby, Dustin Tran, and Mario Lucic. Revisiting the calibration of modern neural networks. *Advances in Neural Information Processing Systems*, 34, 2021.
- Jishnu Mukhoti, Viveka Kulharia, Amartya Sanyal, Stuart Golodetz, Philip Torr, and Puneet Dokania. Calibrating deep neural networks using focal loss. *Advances in Neural Information Processing Systems*, 33:15288–15299, 2020.
- Rafael Müller, Simon Kornblith, and Geoffrey E Hinton. When does label smoothing help? *Advances in neural information processing systems*, 32, 2019.
- Mahdi Pakdaman Naeini, Gregory Cooper, and Milos Hauskrecht. Obtaining well calibrated probabilities using bayesian binning. In *Twenty-Ninth AAAI Conference on Artificial Intelligence*, 2015.
- Jeremy Nixon, Michael W Dusenberry, Linchuan Zhang, Ghassen Jerfel, and Dustin Tran. Measuring calibration in deep learning. In *CVPR Workshops*, volume 2, 2019.
- John Platt et al. Probabilistic outputs for support vector machines and comparisons to regularized likelihood methods. *Advances in large margin classifiers*, 10(3):61–74, 1999.
- Sina Shafaei, Stefan Kugele, Mohd Hafeez Osman, and Alois Knoll. Uncertainty in machine learning: A safety perspective on autonomous driving. In *International Conference on Computer Safety, Reliability, and Security*, pp. 458–464. Springer, 2018.

- Junjiao Tian, Dylan Yung, Yen-Chang Hsu, and Zsolt Kira. A geometric perspective towards neural calibration via sensitivity decomposition. *Advances in Neural Information Processing Systems*, 34, 2021.
- Ilya O Tolstikhin, Neil Houlsby, Alexander Kolesnikov, Lucas Beyer, Xiaohua Zhai, Thomas Unterthiner, Jessica Yung, Andreas Steiner, Daniel Keysers, Jakob Uszkoreit, et al. Mlp-mixer: An all-mlp architecture for vision. *Advances in Neural Information Processing Systems*, 34:24261–24272, 2021.
- Jiancheng Yang, Rui Shi, Donglai Wei, Zequan Liu, Lin Zhao, Bilian Ke, Hanspeter Pfister, and Bingbing Ni. Medmnist v2-a large-scale lightweight benchmark for 2d and 3d biomedical image classification. *Scientific Data*, 10(1):41, 2023.
- Sergey Zagoruyko and Nikos Komodakis. Wide residual networks. *arXiv preprint arXiv:1605.07146*, 2016.

Appendix

A Algorithmic Descriptions of Neural Clamping

Algorithm 1 Neural Clamping

- 1: **Input:** Fixed K -way image classifier $f_\theta(\cdot)$, calibration dataset $\{\mathbf{x}_i, y_i\}_{i=1}^n$, learning rate ϵ , focal loss hyperparameter γ , and weight-decay regularization hyperparameter λ
 - 2: **Output:** The optimal input perturbation δ and temperature T
 - 3: **Initialize**
 $\delta \leftarrow$ initialization (random or data-driven)
 $T \leftarrow 1$
 $Loss \leftarrow \mathcal{L}_{FL}^\gamma$ and λ according to equation 9
 - 4: **while** not converged **do**
 - 5: Sample data batch $\text{batches}(\mathbf{x}_i, y_i) \sim \{\mathbf{x}_i, y_i\}_{i=1}^n$
 - 6: **for** $\text{batches}(\mathbf{x}_i, y_i)$ **do**
 - 7: Update $\delta \leftarrow \delta - \epsilon \nabla_\delta Loss(f_\theta(\mathbf{x}_i + \delta)/T, y_i)$
 - 8: Update $T \leftarrow T - \epsilon \nabla_T Loss(f_\theta(\mathbf{x}_i + \delta)/T, y_i)$
 - 9: **end for**
 - 10: **end while**
 - 11: **return** δ, T
-

In our implementation, we set the hyperparameters λ and γ in equation (9) by the best parameter minimizing the ECE on the calibration dataset. The selection of λ/γ sweeps from 0.001 to 10 and 0.01 to 5. with an increment of 0.001/0.01, respectively.

The input calibration parameter δ and the output calibration parameter T are optimized using the stochastic gradient descent (SGD) optimizer with learning rate 0.001, batch size 512, and 100 epochs. For initialization, δ use randomly initialized (Gaussian distribution with mean=0 and variance=0.01) and T is set to 1.

B Proof for Lemma 3.1

Lemma 3.1 (optimality of joint input-output calibration) *For any input perturbation δ , let $f_\theta(\cdot) = [f_\theta^{(1)}, \dots, f_\theta^{(K)}]$ be a fixed K -way neural network classifier and let \mathbf{z} be the output logits of a perturbed data input $\mathbf{x} + \delta$. Then the proposed form of joint input-output calibration in Neural Clamping is the unique solution $q^*(\mathbf{z})^{(k)} = \frac{\exp[f_\theta^{(k)}(\mathbf{x} + \delta)/T]}{\sum_{j=1}^K \exp[f_\theta^{(j)}(\mathbf{x} + \delta)/T]}$, $\forall k \in \{1, \dots, K\}$, to the constrained entropy maximization problem in equation 7.*

Proof. Without loss of generality, the following proof assumes a vectorized input dimension. Our proof extends the theoretical analysis on temperature scaling in the supplementary materials S.2 of Guo et al. (2017) to consider an input perturbation δ . We use the method of Lagrange multipliers to solve the constrained entropy maximization problem in equation 7. Let $\lambda_0 \in \mathbb{R}$ and $\lambda_1, \lambda_2, \dots, \lambda_n \in \mathbb{R}$ be the Lagrangian multipliers for the constraint $\sum_{i=1}^n \mathbf{z}_i^\top \mathbf{e}^{(y_i)} = \sum_{i=1}^n \mathbf{z}_i^\top q(\mathbf{z}_i)$ and $\sum_{i=1}^n \mathbf{1}^\top q(\mathbf{z}_i) = 1$, $\forall i$, respectively. We will show the optimal solution automatically satisfies the first constraint (nonnegativity) $q(\mathbf{z}_i)^{(k)} \geq 0$ for all i and k later. Then we define

$$\begin{aligned}
 L = & - \sum_{i=1}^n q(\mathbf{z}_i)^\top \log(q(\mathbf{z}_i)) + \lambda_0 \sum_{i=1}^n \left[\mathbf{z}_i^\top q(\mathbf{z}_i) - \mathbf{z}_i \cdot \mathbf{e}^{(y_i)} \right] \\
 & + \sum_{i=1}^n \lambda_i \left[\mathbf{1}^\top q(\mathbf{z}_i) - 1 \right]
 \end{aligned} \tag{10}$$

Taking the partial derivative of L with respect to $q(\mathbf{z}_i)$ gives

$$\frac{\partial}{\partial q(\mathbf{z}_i)} L = -\log(q(\mathbf{z}_i)) - \mathbf{1} + \lambda_0 \mathbf{z}_i + \lambda_i \mathbf{1} \tag{11}$$

Let the partial derivative of L equal 0, then we can get

$$q(\mathbf{z}_i) = \begin{bmatrix} \exp[\lambda_0 z_i^{(1)} + \lambda_i - 1] \\ \vdots \\ \exp[\lambda_0 z_i^{(K)} + \lambda_i - 1] \end{bmatrix} \quad (12)$$

Note that this expression suggests $q(\mathbf{z}_i)^{(k)} \geq 0$ and thus the first constraint is satisfied. Due to the constraint $\sum_{i=1}^n \mathbf{1}^\top q(\mathbf{z}_i) = 1$ for all i , the solution $q(z_i)$ must be

$$q(z_i)^{(k)} = \frac{\exp[\lambda_0 z_i^{(k)}]}{\sum_{j=1}^K \exp[\lambda_0 z_i^{(j)}]} \quad (13)$$

By setting $T = \frac{1}{\lambda_0}$, we can get the unique solution

$$q^*(\mathbf{z})^{(k)} = \frac{\exp[f_\theta^{(k)}(\mathbf{x} + \boldsymbol{\delta})/T]}{\sum_{j=1}^K \exp[f_\theta^{(j)}(\mathbf{x} + \boldsymbol{\delta})/T]}, \quad \forall k \in \{1, \dots, K\}. \quad (14)$$

□

C Proof for Theorem 3.2

Theorem 3.2 (provable entropy increment and data-driven initialization) *Let $[\boldsymbol{\alpha}, \boldsymbol{\beta}]$ be the feasible range of data inputs and $\mathbf{g} = \sum_{i=1}^n \mathbf{g}_i = [g^{(1)}, \dots, g^{(K)}]$ be the sum of local input gradients. Define $\boldsymbol{\eta} \in \mathbb{R}^m$ element-wise such that $\eta_j = \ell_j - \alpha_j$ if $g^{(j)} < 0$, $\eta_j = \beta_j - \mu_j$ if $g^{(j)} > 0$, and $\eta_j = 0$ otherwise, for every $j \in \{1, \dots, m\}$. Approaching by first-order approximation and given the same temperature value T , Neural Clamping increases the entropy of temperature scaling by $\boldsymbol{\delta}^\top \mathbf{g}$. Furthermore, the optimal value $\tilde{\boldsymbol{\delta}}$ for maximizing $\boldsymbol{\delta}^\top \mathbf{g}$ is $\tilde{\boldsymbol{\delta}} = \text{sign}(\mathbf{g}) \odot \boldsymbol{\eta}$.*

Proof. For ease of understanding, let $\hat{H}(\mathbf{x}) = H(\sigma(f_\theta(\mathbf{x})/T))$ denote the entropy of the classifier f_θ (with softmax as the final output layer) after calibration. We have Taylor series expansion of \hat{H} at a point \mathbf{x}_0 as:

$$\begin{aligned} \hat{H}(\mathbf{x}) &= \hat{H}(\mathbf{x}_0) + (\mathbf{x} - \mathbf{x}_0)^\top \nabla \hat{H}(\mathbf{x}_0) \\ &\quad + \frac{1}{2} (\mathbf{x} - \mathbf{x}_0)^\top \nabla^2 \hat{H}(\mathbf{x}_0) (\mathbf{x} - \mathbf{x}_0) + \dots \end{aligned} \quad (15)$$

Adding input perturbation $\boldsymbol{\delta}$ to input data point \mathbf{x} and applying the first-order approximation on $\hat{H}(\mathbf{x})$, we can get

$$\begin{aligned} \hat{H}(\mathbf{x} + \boldsymbol{\delta}) &= \hat{H}(\mathbf{x}) + [(\mathbf{x} + \boldsymbol{\delta}) - \mathbf{x}]^\top \nabla \hat{H}(\mathbf{x}) + \dots \\ &\approx \hat{H}(\mathbf{x}) + \boldsymbol{\delta}^\top \nabla \hat{H}(\mathbf{x}) \end{aligned} \quad (16)$$

Then we can use above approximation to compute the average output entropy for all data $\{\mathbf{x}_i\}_{i=1}^n$:

$$\frac{1}{n} \sum_{i=1}^n \hat{H}(\mathbf{x}_i + \boldsymbol{\delta}) = \frac{1}{n} \sum_{i=1}^n \hat{H}(\mathbf{x}_i) + \frac{1}{n} \sum_{i=1}^n \boldsymbol{\delta}^\top \nabla \hat{H}(\mathbf{x}_i) \quad (17)$$

Let $\mathbf{g}_i = \nabla \hat{H}(\mathbf{x}_i) = \nabla H(\sigma(f_\theta(\mathbf{x}_i)/T))$ is the input gradient with respect to \mathbf{x}_i , and \mathbf{g} is the average input gradient $\frac{1}{n} \sum_{i=1}^n \mathbf{g}_i$. The first term is the original entropy value, namely the entropy of temperature scaling. The second term is the additional entropy term caused by introducing the input perturbation. The latter can be rewritten as:

$$\Delta \hat{H}(\mathbf{x}_i + \boldsymbol{\delta}) = \frac{1}{n} \sum_{i=1}^n \boldsymbol{\delta}^\top \nabla \hat{H}(\mathbf{x}_i) = \frac{\boldsymbol{\delta}^\top}{n} \sum_{i=1}^n \mathbf{g}_i = \boldsymbol{\delta}^\top \mathbf{g} \quad (18)$$

Therefore, Neural Clamping increases the entropy of temperature scaling by $\delta^\top \mathbf{g}$.

Maximizing the scalar product $\delta^\top \mathbf{g}$ under the constraint $\mathbf{x}_i + \delta \in [\alpha, \beta]$ for all i is equivalent to maximizing an inner product over an L_∞ ball, where $[\alpha, \beta] \subset \mathbb{R}^m \times \mathbb{R}^m$ means the bounded range of all feasible data inputs, e.g., every image pixel value is within $[0, 255]$.

Due to the constraint, we further define $\ell \in \mathbb{R}^m$ and $\mu \in \mathbb{R}^m$ as the lower bound and the upper bound over all calibration data $\{\mathbf{x}_i\}_{i=1}^n$ on each input dimension. That is, their j -th entry is defined as $\ell_j = \min_{i \in \{1, \dots, n\}} x_i^{(j)}$ and $\mu_j = \max_{i \in \{1, \dots, n\}} x_i^{(j)}$, respectively. Then we can find available range value $\eta \in \mathbb{R}^m$ for δ to maximize the scalar product $\delta^\top \mathbf{g}$ according to the direction of input gradient, η can be defined as:

$$\eta_j = \begin{cases} \ell_j - \alpha_j & \text{if } g^{(j)} < 0 \\ \beta_j - \mu_j & \text{if } g^{(j)} > 0 \\ 0 & \text{otherwise} \end{cases} \quad (19)$$

Finally, we can get the optimal $\tilde{\delta}$ for maximizing the scalar product $\delta^\top \mathbf{g}$, i.e.,

$$\tilde{\delta} = \text{sign}(\mathbf{g}) \odot \eta \quad (20)$$

□

D Result with Varying Bin Numbers

Calibration error measurements are known to be influenced by the number of bins. In order to account for the influence of bin numbers on calibration error measurements, we present additional results using different bin configurations. Specifically, we evaluate the results of the BloodMNIST experiment with bin numbers 10 and 20, which are displayed in Table 5 and Table 6, respectively. Furthermore, we provide the results of the CIFAR-100 experiment with bin numbers 10 and 20 in Table 7 and Table 8, respectively. Lastly, the results of the ImageNet-1K experiment with bin numbers 10 and 20 can be found in Table 9 and Table 10, respectively. By examining the results across different bin configurations, we gain a more comprehensive understanding of the performance of our approach in different scenarios.

Table 5: Comparison with various calibration methods on BloodMNIST with ResNet-50 (calibration metric bins=10). The reported results are mean and standard deviation over 5 runs. The best/second-best method is highlighted by blue/green color. On ECE/AECE, the relative improvement of Neural Clamping to the best baseline is 21% and 28%, respectively.

ResNet-50					
Method	Accuracy (%)	Entropy \uparrow	ECE (%) \downarrow	AECE (%) \downarrow	SCE ($\times 10^{-2}$) \downarrow
Uncalibration	85.79	0.2256	5.77	5.76	1.6217
Temp. Scaling	85.79 ± 0	0.3726 ± 0	1.32 ± 0	1.43 ± 0	1.0148 ± 0
TS by Grid Search	85.79 ± 0	0.3726 ± 0	1.86 ± 0	1.59 ± 0	1.0134 ± 0
Vector Scaling	85.79 ± 0.05	0.3653 ± 0.0023	1.80 ± 0.09	1.87 ± 0.17	0.8355 ± 0.0688
Matrix Scaling	85.79 ± 0.38	0.2984 ± 0.0161	4.93 ± 0.67	4.85 ± 0.72	1.3964 ± 0.1345
MS-ODIR	85.79 ± 0.04	0.3726 ± 0.0001	1.59 ± 0.03	1.65 ± 0.05	0.7277 ± 0.0021
Dir-ODIR	85.79 ± 0.02	0.3748 ± 0.0002	1.94 ± 0.07	1.39 ± 0.04	0.7435 ± 0.0141
NC (CE)	85.79 ± 0.02	0.3820 ± 0.0005	1.20 ± 0.04	1.32 ± 0.04	1.0131 ± 0.0063
NC (FL)	85.82 ± 0.03	0.4204 ± 0.0004	1.04 ± 0.04	0.99 ± 0.04	0.9744 ± 0.0031

E Reliability Diagrams

To visually compare the ECE results (15 bins) to each method with the groundtruth, we present reliability diagrams. These diagrams offer a comprehensive view of the calibration performance. The reliability diagrams of BloodMNIST, CIFAR-100, and ImageNet are presented in Figure 4, Figure 5, and Figure 6,

Table 6: Comparison with various calibration methods on BloodMNIST with ResNet-50 (calibration metric bins=20). The reported results are mean and standard deviation over 5 runs. The best/second-best method is highlighted by blue/green color. On ECE/AECE, the relative improvement of Neural Clamping to the best baseline is 26% and 22%, respectively.

ResNet-50					
Method	Accuracy (%)	Entropy \uparrow	ECE (%) \downarrow	AECE (%) \downarrow	SCE ($\times 10^{-2}$) \downarrow
Uncalibration	85.79	0.2256	5.77	5.76	1.7247
Temp. Scaling	85.79 ± 0	0.3726 ± 0	1.62 ± 0	1.49 ± 0	1.1978 ± 0
TS by Grid Search	85.79 ± 0	0.3726 ± 0	2.00 ± 0	1.66 ± 0	1.1644 ± 0
Vector Scaling	85.79 ± 0.05	0.3653 ± 0.0023	2.11 ± 0.15	2.09 ± 0.10	1.0276 ± 0.0798
Matrix Scaling	85.79 ± 0.38	0.2984 ± 0.0161	5.00 ± 0.63	4.94 ± 0.66	1.5581 ± 0.1318
MS-ODIR	85.79 ± 0.04	0.3726 ± 0.0001	2.08 ± 0.06	2.32 ± 0.06	0.9422 ± 0.0107
Dir-ODIR	85.79 ± 0.02	0.3748 ± 0.0002	2.05 ± 0.07	1.50 ± 0.02	0.9563 ± 0.0206
NC (CE)	85.79 ± 0.02	0.3820 ± 0.0005	1.83 ± 0.13	1.43 ± 0.05	1.2076 ± 0.0116
NC (FL)	85.82 ± 0.03	0.4204 ± 0.0004	1.19 ± 0.08	1.17 ± 0.06	1.1905 ± 0.0031

respectively. Pink color is the perfectly calibrated, and purple color is the actual probability of the output. By examining these diagrams, we gain graphical insights into the effectiveness of each method’s calibration performance.

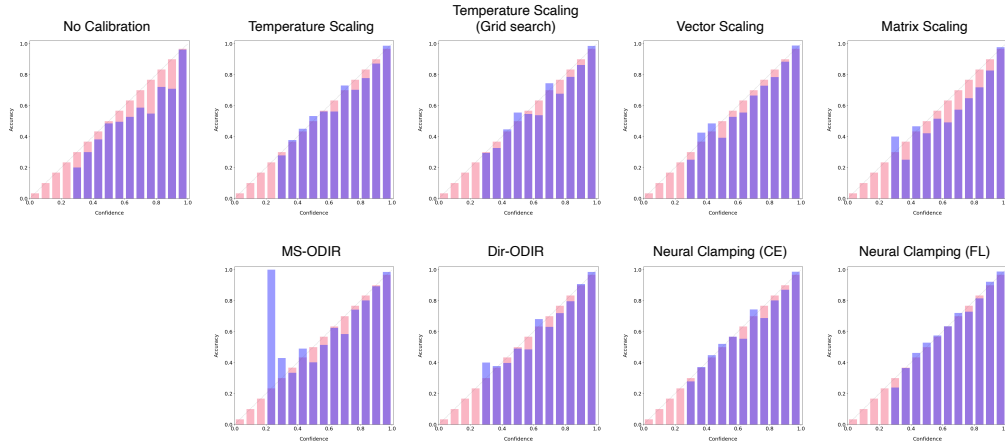


Figure 4: Reliability diagram of ResNet-50 on BloodMNIST with 15 bins ECE metric

F Computationally Efficient Neural Clamping

We utilize our Theorem 1 to develop a Computationally Efficient Neural Clamping approach, referred to as NC (Eff.). NC (Eff.) adopts the data-driven initialization δ for the input perturbation (input gradient w.r.t. entropy as discussed in Sec. 3.4), followed by temperature scaling (TS) with grid search (TS-Grid). This lightweight version spares the need for training input perturbation, requires only one additional backpropagation, and does not add additional hyperparameter tuning.

To demonstrate the effectiveness of NC (Eff.), we present two examples: ResNet-50 on BloodMNIST and ResNet-110 on CIFAR-100, in Table 11. We observed similar results across other examples as well. In our paper, the resolution for temperature scaling (grid search) was set to 0.001, and we included a comparison group with a resolution of 0.01 for analysis purposes. The table clearly shows that regardless of the resolution used, NC (Eff.) consistently outperforms temperature scaling (grid search) in terms of ECE, with improvements of up to 33.7 %. Notably, even with lower resolution, NC (Eff.) can still achieve better results than high-resolution temperature scaling in terms of both speed and ECE.

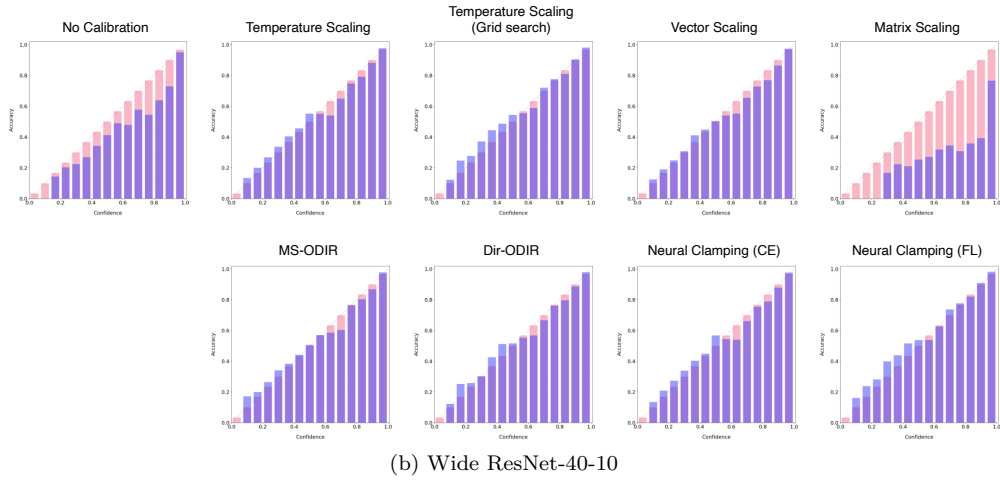
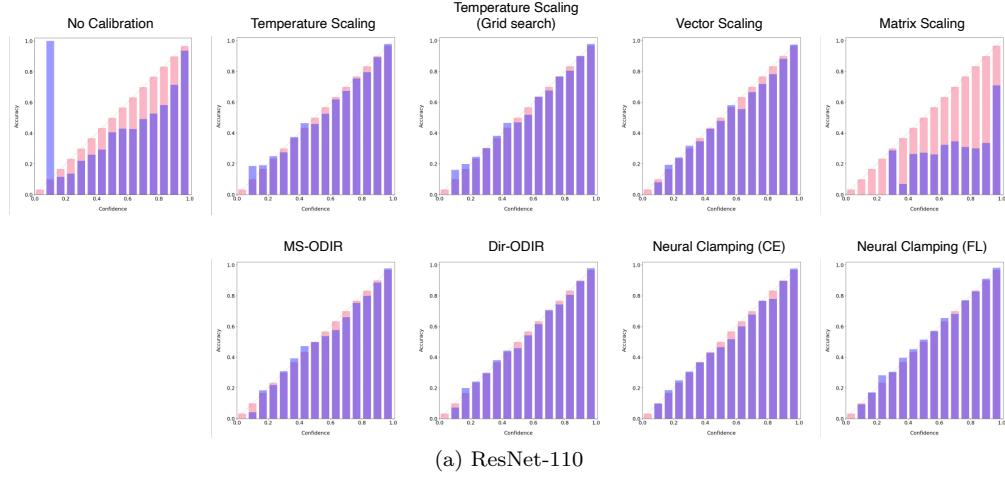


Figure 5: Reliability diagram of (a) ResNet-110 and (b) Wide ResNet-40-10 on CIFAR-100 with 15 bins ECE metric

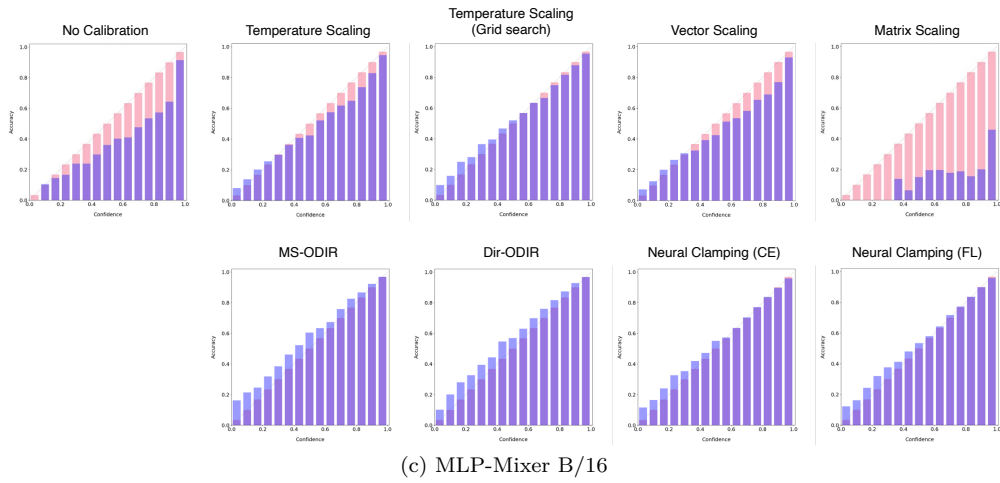
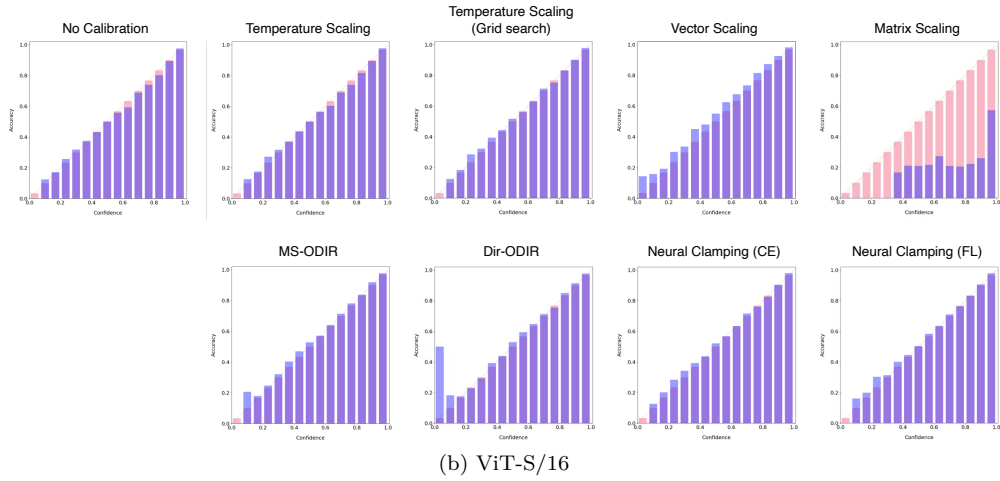
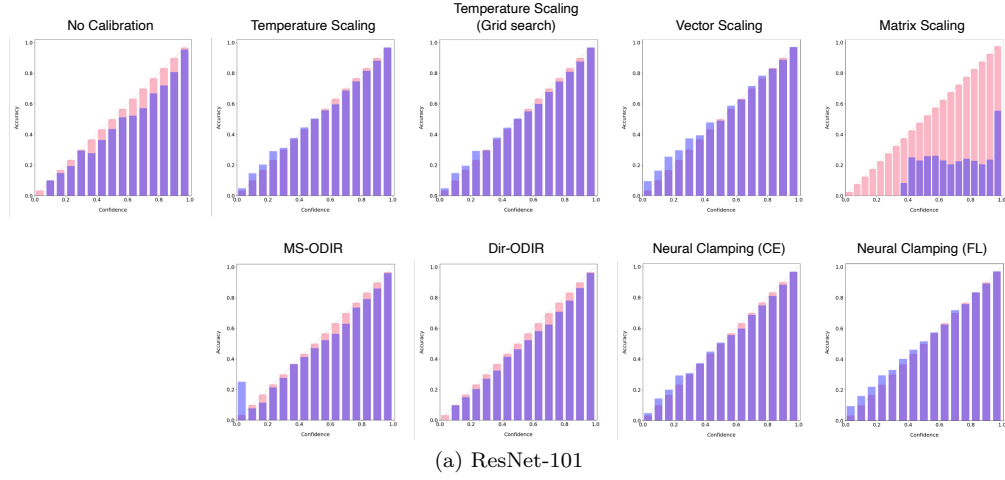


Figure 6: Reliability diagram of (a) ResNet-101, (b) ViT-S/16, and (c) MLP-Mixer B/16 on ImageNet with 15 bins ECE metric

Table 7: Comparison with various calibration methods on CIFAR-100 with different models (calibration metric bins=10). The reported results are mean and standard deviation over 5 runs. The best/second-best method is highlighted by blue/green color. On ECE, the relative improvement of Neural Clamping to the best baseline is 26/2 % on ResNet-110/Wide ResNet-40-10, respectively.

ResNet-110					
Method	Accuracy (%)	Entropy \uparrow	ECE (%) \downarrow	AECE (%) \downarrow	SCE ($\times 10^{-2}$) \downarrow
Uncalibration	74.15	0.47430	10.707	10.714	0.26065
Temperature Scaling	74.15 ± 0	0.8991 ± 0	1.37 ± 0	1.48 ± 0	0.1443 ± 0
TS by Grid Search	74.15 ± 0	0.9239 ± 0	1.08 ± 0	1.26 ± 0	0.1425 ± 0
Vector Scaling	73.81 ± 0.05	0.8698 ± 0.0008	2.16 ± 0.14	2.13 ± 0.18	0.1683 ± 0.0031
Matrix Scaling	62.03 ± 0.31	0.1552 ± 0.0026	31.86 ± 0.29	31.85 ± 0.29	0.6749 ± 0.0060
MS-ODIR	74.07 ± 0.03	0.9035 ± 0.0001	1.67 ± 0.04	1.79 ± 0.03	0.1555 ± 0.0009
Dir-ODIR	74.10 ± 0.04	0.9160 ± 0.0002	1.16 ± 0.03	1.19 ± 0.08	0.1501 ± 0.0008
Neural Clamping (CE)	74.17 ± 0.07	0.8928 ± 0.0061	1.60 ± 0.19	1.50 ± 0.11	0.1427 ± 0.0012
Neural Clamping (FL)	74.16 ± 0.09	0.9707 ± 0.0049	0.80 ± 0.12	0.86 ± 0.07	0.1486 ± 0.0015
Wide-ResNet-40-10					
Method	Accuracy (%)	Entropy \uparrow	ECE (%) \downarrow	AECE (%) \downarrow	SCE ($\times 10^{-2}$) \downarrow
Uncalibration	79.51	0.4211	7.63	7.63	0.2009
Temperature Scaling	79.51 ± 0	0.7421 ± 0	2.17 ± 0	2.18 ± 0	0.1369 ± 0
TS by Grid Search	79.51 ± 0	0.8359 ± 0	1.65 ± 0	1.48 ± 0	0.1417 ± 0
Vector Scaling	79.08 ± 0.09	0.7079 ± 0.0012	2.49 ± 0.08	2.33 ± 0.07	0.1612 ± 0.0033
Matrix Scaling	68.48 ± 0.16	0.1372 ± 0.0023	26.14 ± 0.14	26.13 ± 0.15	0.5563 ± 0.0020
MS-ODIR	79.15 ± 0.03	0.7529 ± 0.0002	1.90 ± 0.04	1.95 ± 0.03	0.1501 ± 0.0005
Dir-ODIR	79.51 ± 0.02	0.7707 ± 0.0001	1.74 ± 0.02	1.98 ± 0.01	0.1366 ± 0.0007
Neural Clamping (CE)	79.53 ± 0.01	0.7462 ± 0.0030	2.15 ± 0.06	2.22 ± 0.03	0.1368 ± 0.0003
Neural Clamping (FL)	79.53 ± 0.04	0.8626 ± 0.0033	1.61 ± 0.10	1.61 ± 0.10	0.1445 ± 0.0008

Table 8: Comparison with various calibration methods on CIFAR-100 with different models (calibration metric bins=20). The reported results are mean and standard deviation over 5 runs. The best/second-best method is highlighted by blue/green color. On ECE, the relative improvement of Neural Clamping to the best baseline is 26/6 % on ResNet-110/Wide ResNet-40-10, respectively.

ResNet-110					
Method	Accuracy (%)	Entropy \uparrow	ECE (%) \downarrow	AECE (%) \downarrow	SCE ($\times 10^{-2}$) \downarrow
Uncalibration	74.15	0.4743	10.74	10.71	0.2937
Temperature Scaling	74.15 ± 0	0.8991 ± 0	1.72 ± 0	1.68 ± 0	0.1943 ± 0
TS by Grid Search	74.15 ± 0	0.9240 ± 0	1.62 ± 0	1.51 ± 0	0.1938 ± 0
Vector Scaling	73.81 ± 0.05	0.8699 ± 0.0008	2.31 ± 0.19	2.25 ± 0.21	0.2155 ± 0.0027
Matrix Scaling	62.03 ± 0.31	0.1552 ± 0.0026	31.86 ± 0.29	31.86 ± 0.29	0.6914 ± 0.0060
MS-ODIR	74.07 ± 0.03	0.9035 ± 0.0001	1.89 ± 0.08	1.82 ± 0.02	0.2031 ± 0.0010
Dir-ODIR	74.10 ± 0.04	0.9160 ± 0.0002	1.48 ± 0.07	1.44 ± 0.20	0.2046 ± 0.0020
Neural Clamping (CE)	74.17 ± 0.07	0.8929 ± 0.0061	1.78 ± 0.18	1.62 ± 0.12	0.1937 ± 0.0029
Neural Clamping (FL)	74.16 ± 0.09	0.9941 ± 0.0049	1.09 ± 0.16	1.20 ± 0.17	0.2003 ± 0.0029
Wide-ResNet-40-10					
Method	Accuracy (%)	Entropy \uparrow	ECE (%) \downarrow	AECE (%) \downarrow	SCE ($\times 10^{-2}$) \downarrow
Uncalibration	79.51	0.4211	7.63	7.63	0.2351
Temperature Scaling	79.51 ± 0	0.7421 ± 0	2.22 ± 0	2.21 ± 0	0.1818 ± 0
TS by Grid Search	79.51 ± 0	0.8359 ± 0	1.74 ± 0	1.75 ± 0	0.1900 ± 0
Vector Scaling	79.08 ± 0.09	0.7079 ± 0.0012	2.59 ± 0.09	2.47 ± 0.08	0.2020 ± 0.0032
Matrix Scaling	68.48 ± 0.16	0.1372 ± 0.0023	26.14 ± 0.14	26.13 ± 0.15	0.5728 ± 0.0013
MS-ODIR	79.15 ± 0.03	0.7529 ± 0.0002	1.95 ± 0.04	1.96 ± 0.03	0.1915 ± 0.0006
Dir-ODIR	79.51 ± 0.01	0.7707 ± 0.0001	1.94 ± 0.02	1.99 ± 0.01	0.1834 ± 0.0008
Neural Clamping (CE)	79.53 ± 0.01	0.7462 ± 0.0030	2.20 ± 0.03	2.24 ± 0.04	0.1816 ± 0.0003
Neural Clamping (FL)	79.53 ± 0.04	0.8626 ± 0.0033	1.63 ± 0.06	1.70 ± 0.14	0.1916 ± 0.0019

Table 9: Comparison with various calibration methods on ImageNet with different models (calibration metric bins=10). The reported results are mean and standard deviation over 5 runs. The best/second-best method is highlighted by blue/green color. On ECE, the relative improvement of Neural Clamping to the best baseline is 17/1/11 % on ResNet-101/ViT-S16/MLP-Mixer B16, respectively.

ResNet-101					
Method	Accuracy (%)	Entropy \uparrow	ECE (%) \downarrow	AECE (%) \downarrow	SCE ($\times 10^{-3}$) \downarrow
Uncalibration	75.73	0.6608	5.88	5.88	0.2808
Temperature Scaling	75.73 ± 0	0.9376 ± 0	1.97 ± 0	1.91 ± 0	0.2677 ± 0
TS by Grid Search	75.73 ± 0	0.9244 ± 0	2.04 ± 0	1.97 ± 0	0.2683 ± 0
Vector Scaling	75.67 ± 0.07	1.0463 ± 0.0017	1.99 ± 0.09	1.91 ± 0.05	0.2775 ± 0.0009
Matrix Scaling	51.97 ± 0.30	0.0593 ± 0.0008	45.60 ± 0.29	45.60 ± 0.28	0.8997 ± 0.0052
MS-ODIR	70.71 ± 0.10	0.9904 ± 0.0016	3.28 ± 0.06	3.28 ± 0.06	0.2990 ± 0.0009
Dir-ODIR	70.72 ± 0.03	0.9841 ± 0.0007	3.47 ± 0.05	3.47 ± 0.05	0.3016 ± 0.0024
Neural Clamping (CE)	75.73 ± 0.01	0.9429 ± 0.0240	1.91 ± 0.16	1.89 ± 0.12	0.2682 ± 0.0004
Neural Clamping (FL)	75.73 ± 0.01	1.0103 ± 0.0245	1.63 ± 0.06	1.62 ± 0.05	0.2700 ± 0.0014
ViT-S/16					
Method	Accuracy (%)	Entropy \uparrow	ECE (%) \downarrow	AECE (%) \downarrow	SCE ($\times 10^{-3}$) \downarrow
Uncalibration	79.90	0.7161	1.28	1.31	0.2460
Temperature Scaling	79.90 ± 0	0.7314 ± 0	1.06 ± 0	1.12 ± 0	0.2462 ± 0
TS by Grid Search	79.90 ± 0	0.7791 ± 0	0.73 ± 0	0.83 ± 0	0.2481 ± 0
Vector Scaling	80.02 ± 0.03	0.9410 ± 0.0014	2.62 ± 0.03	2.68 ± 0.04	0.2598 ± 0.0008
Matrix Scaling	53.99 ± 0.29	0.0646 ± 0.0010	43.36 ± 0.29	43.36 ± 0.29	0.8765 ± 0.0055
MS-ODIR	75.94 ± 0.09	0.9810 ± 0.0018	0.86 ± 0.10	0.90 ± 0.10	0.2722 ± 0.0019
Dir-ODIR	75.93 ± 0.09	0.9788 ± 0.0007	0.86 ± 0.06	0.81 ± 0.08	0.2721 ± 0.0014
Neural Clamping (CE)	79.98 ± 0.01	0.7898 ± 0.0028	0.73 ± 0.02	0.88 ± 0.04	0.2475 ± 0.0004
Neural Clamping (FL)	79.97 ± 0.01	0.7934 ± 0.0038	0.72 ± 0.05	0.79 ± 0.04	0.2474 ± 0.0002
MLP-Mixer B/16					
Method	Accuracy (%)	Entropy \uparrow	ECE (%) \downarrow	AECE (%) \downarrow	SCE ($\times 10^{-3}$) \downarrow
Uncalibration	73.94	0.6812	11.56	11.55	0.3316
Temperature Scaling	73.94 ± 0	1.2735 ± 0	4.92 ± 0	4.91 ± 0	0.2847 ± 0
TS by Grid Search	73.94 ± 0	1.6243 ± 0	2.60 ± 0	2.74 ± 0	0.2844 ± 0
Vector Scaling	73.24 ± 0.06	1.1474 ± 0.0089	6.87 ± 0.17	6.81 ± 0.13	0.3022 ± 0.0017
Matrix Scaling	40.96 ± 0.31	0.1137 ± 0.0010	54.50 ± 0.28	54.50 ± 0.28	1.0897 ± 0.0042
MS-ODIR	73.16 ± 0.02	1.8049 ± 0.0016	4.48 ± 0.03	4.73 ± 0.05	0.3006 ± 0.0011
Dir-ODIR	73.13 ± 0.05	1.8083 ± 0.0013	4.51 ± 0.07	4.75 ± 0.08	0.3009 ± 0.0009
Neural Clamping (CE)	74.14 ± 0.01	1.7952 ± 0.0302	2.51 ± 0.21	2.50 ± 0.18	0.2937 ± 0.0022
Neural Clamping (FL)	74.12 ± 0.01	1.7673 ± 0.0269	2.31 ± 0.16	2.32 ± 0.13	0.2916 ± 0.0016

Table 10: Comparison with various calibration methods on ImageNet with different models (calibration metric bins=20). The reported results are mean and standard deviation over 5 runs. The best/second-best method is highlighted by blue/green color. On ECE, the relative improvement of Neural Clamping to the best baseline is 12/6/12 % on ResNet-101/ViT-S16/MLP-Mixer B16, respectively.

ResNet-101					
Method	Accuracy (%)	Entropy \uparrow	ECE \downarrow	AECE \downarrow	SCE ($\times 10^{-3}$) \downarrow
Uncalibration	75.73	0.6608	5.93	5.88	0.3482
Temperature Scaling	75.73 ± 0	0.9376 ± 0	1.98 ± 0	1.91 ± 0	0.3404 ± 0
TS by Grid Search	75.73 ± 0	0.9244 ± 0	2.09 ± 0	1.97 ± 0	0.3401 ± 0
Vector Scaling	75.67 ± 0.07	1.0463 ± 0.0017	2.05 ± 0.13	1.99 ± 0.08	0.3502 ± 0.0013
Matrix Scaling	51.97 ± 0.30	0.0593 ± 0.0008	45.61 ± 0.28	45.60 ± 0.28	0.9058 ± 0.0053
MS-ODIR	70.71 ± 0.10	0.9904 ± 0.0016	3.29 ± 0.04	3.28 ± 0.06	0.3795 ± 0.0011
Dir-ODIR	70.72 ± 0.03	0.9841 ± 0.0007	3.49 ± 0.05	3.47 ± 0.05	0.3842 ± 0.0017
Neural Clamping (CE)	75.73 ± 0.01	0.9429 ± 0.0240	1.96 ± 0.14	1.89 ± 0.12	0.3405 ± 0.0004
Neural Clamping (FL)	75.73 ± 0.01	1.0103 ± 0.0245	1.74 ± 0.03	1.64 ± 0.03	0.3434 ± 0.0018
ViT-S/16					
Method	Accuracy (%)	Entropy \uparrow	ECE \downarrow	AECE \downarrow	SCE ($\times 10^{-3}$) \downarrow
Uncalibration	79.90	0.7161	1.32	1.31	0.3079
Temperature Scaling	79.90 ± 0	0.7314 ± 0	1.13 ± 0	1.12 ± 0	0.3084 ± 0
TS by Grid Search	79.90 ± 0	0.7791 ± 0	0.88 ± 0	0.97 ± 0	0.3101 ± 0
Vector Scaling	80.02 ± 0.03	0.9410 ± 0.0014	2.62 ± 0.03	2.72 ± 0.03	0.3269 ± 0.0012
Matrix Scaling	53.99 ± 0.29	0.0646 ± 0.0010	43.36 ± 0.29	43.36 ± 0.29	0.8835 ± 0.0056
MS-ODIR	75.94 ± 0.09	0.9810 ± 0.0018	0.92 ± 0.09	0.98 ± 0.09	0.3504 ± 0.0022
Dir-ODIR	75.93 ± 0.09	0.9788 ± 0.0007	0.97 ± 0.09	0.91 ± 0.10	0.3485 ± 0.0016
Neural Clamping (CE)	79.98 ± 0.01	0.7898 ± 0.0028	0.82 ± 0.10	1.00 ± 0.08	0.3115 ± 0.0005
Neural Clamping (FL)	79.97 ± 0.01	0.7934 ± 0.0038	0.84 ± 0.09	0.91 ± 0.01	0.3117 ± 0.0004
MLP-Mixer B/16					
Method	Accuracy (%)	Entropy \uparrow	ECE \downarrow	AECE \downarrow	SCE ($\times 10^{-3}$) \downarrow
Uncalibration	73.94	0.6812	11.56	11.55	0.3781
Temperature Scaling	73.94 ± 0	1.2735 ± 0	5.04 ± 0	4.91 ± 0	0.3450 ± 0
TS by Grid Search	73.94 ± 0	1.6243 ± 0	2.71 ± 0	2.74 ± 0	0.3553 ± 0
Vector Scaling	73.24 ± 0.06	1.1474 ± 0.0089	6.91 ± 0.17	6.84 ± 0.13	0.3552 ± 0.0017
Matrix Scaling	40.96 ± 0.31	0.1137 ± 0.0010	54.50 ± 0.28	54.50 ± 0.28	1.1024 ± 0.0042
MS-ODIR	73.16 ± 0.02	1.8049 ± 0.0016	4.71 ± 0.08	4.73 ± 0.05	0.3821 ± 0.0018
Dir-ODIR	73.13 ± 0.05	1.8083 ± 0.0013	4.73 ± 0.09	4.77 ± 0.09	0.3821 ± 0.0011
Neural Clamping (CE)	74.14 ± 0.01	1.7952 ± 0.0302	2.55 ± 0.18	2.53 ± 0.18	0.3672 ± 0.0028
Neural Clamping (FL)	74.12 ± 0.01	1.7673 ± 0.0269	2.36 ± 0.13	2.36 ± 0.13	0.3644 ± 0.0021

Table 11: Time comparison with Computationally Efficient Neural Clamping (NC (Eff.)) and temperature scaling by grid search.

ResNet-50 on BloodMNIST					
Method	Resolution	Acc. (%)	Entropy \uparrow	ECE (%) \downarrow	Time (s)
Uncalibration	N/A	85.79	0.2256	5.77	N/A
TS-Grid	0.01	85.79	0.3654	2.16	1.5
TS-Grid	0.001	85.79	0.3684	2.13	11.9
NC (Eff.)	0.01	85.79	0.3953	1.47	5.8
NC (Eff.)	0.001	85.79	0.3953	1.43	16.2
NC (FL)	N/A	85.79	0.4204	1.05	35.0
ResNet-110 on CIFAR-100					
Method	Resolution	Acc. (%)	Entropy \uparrow	ECE (%) \downarrow	Time (s)
Uncalibration	N/A	74.15	0.4742	10.74	N/A
TS-Grid	0.01	74.15	0.9268	1.36	2.2
TS-Grid	0.001	74.15	0.9239	1.35	13.0
NC (Eff.)	0.01	74.19	0.9371	1.23	7.2
NC (Eff.)	0.001	74.19	0.9342	1.23	18.0
NC (FL)	N/A	74.16	0.9707	0.89	227.0